Modeling unsteady turbulent flows over ripples: Reynolds-averaged Navier-Stokes equations (RANS) versus large-eddy simulation (LES)

Yeon S. Chang[1] and Alberto Scotti

Department of Marine Sciences, University of North Carolina, Chapel Hill, North Carolina, USA

Received 17 November 2003; accepted 6 July 2004; published 24 September 2004.

[1] In this paper we consider the problem of modeling a turbulent pulsating boundary layer over ripples. We compare the results of two modeling strategies, Wilcox's $k - \omega$ Reynolds-Averaged Navier-Stokes equations (RANS) and large-eddy simulation (LES) employing the Lagrangian dynamic eddy viscosity model. The geometry and parameters employed are relevant to nearshore oceanic flows, and the results are discussed in relation to the problem of sediment transport. Generally, RANS and LES agree well only with regard to the vertical profiles of the streamwise component of the velocity. Large discrepancies were found in all the other quantities considered (e.g., vertical velocity, turbulent kinetic energy, and Reynolds stress). In particular, RANS severely underpredicted the magnitude of the Reynolds stress and overpredicted the amplitude of the oscillations in the vertical velocity. We also found that often the trends exhibited by RANS and LES when the frequency and/or amplitude of the driving conditions was varied were at odds. Since comparison with available experiments indicates that LES is able to accurately model this kind of flows, we conclude that the RANS model is not appropriate to model the suspension and transport of sediment under conditions similar to the ones presented in this study. *INDEX TERMS:* 4568 Oceanography: Physical: Turbulence, diffusion, and mixing processes; 4558 Oceanography: Physical: Sediment transport; 3210 Mathematical Geophysics: Modeling; 3220 Mathematical Geophysics: Nonlinear dynamics; 3230 Mathematical Geophysics: Numerical solutions; *KEYWORDS:* turbulence, numerical modeling, sediment transport

Citation: Chang, Y. S., and A. Scotti (2004), Modeling unsteady turbulent flows over ripples: Reynolds-averaged Navier-Stokes equations (RANS) versus large-eddy simulation (LES), *J. Geophys. Res.*, *109*, C09012, doi:10.1029/2003JC002208.

1. Introduction

[2] The transport of sediments over the continental shelf is an important topic in coastal studies. Examples of applications include transport of particulate organic matter and man-made contaminants; prediction of the optical properties of the water column; prediction of coastal flooding and erosion; evaluation of habitat of commercial fisheries; design of intakes and outfalls of sewage treatment plant and cooling systems.

[3] In shallow waters, two factors contribute to making the problem difficult to analyze: (i) the orbital motion induced by surface gravity waves generates an oscillating boundary layer of thickness $\delta = O(10\text{ cm})$, embedded in the thicker boundary layer generated by low-frequency currents (the Wave Boundary Layer (WBL)), and (ii) the fact that the geometry of the bottom is not known a priori, but is a function of the environmental conditions. At small scales, under the combined effect of waves and currents, a sandy seabed can be flat or corrugated by small, wave-induced sand ripples, while at larger scales [O(100 m)] sand dunes are often present.

[4] In this paper, we focus on the problem of unsteady flows over small-scale ripples. With few exceptions [*Zedler and Street*, 2001, 2002; *Vittori*, 2003; *Gotoh et al.*, 1993, 1994, 1995], the standard approach is to model the fluid phase with Reynolds Averaged Navier-Stokes equations (RANS), while for the particulate phase one usually writes an equation for the Suspended Sediment Concentration (SSC). One such model is the one developed by *Wikramanayake* [1993]. The model assumes that the wave-current boundary layer can be divided into three layers. In the bottom and top layer, the eddy diffusivity is allowed to vary linearly with height, while in the middle layer it is kept constant. Appropriate friction velocities are used in each layer after the theory of *Grant and Madsen* [1979] for the wave-current boundary layer. The equation for the concentration profile can be solved analytically (up to quadratures). *Lee and Hanes* [1996] used it to model the concentration of sediment measured in the field both under low-energy waves over ripples and high-energy waves over sheet flow. The diffusive model gave marginally satisfying results under high-energy waves, while grossly underestimated the profiles under low-energy waves. The addition of

[1]Now at Department of Meteorology and Physical Oceanography, Rosenstiel School of Marine and Atmospheric Science, University of Miami, Miami, Florida, USA.

0148-0227/04/2003JC002208$09.00

Table 1. Parameters Used in the $k-\omega$ Model

σ^*	β^*	σ	γ	β
$\frac{1}{2}$	$\frac{9}{100}$	$\frac{1}{2}$	$\frac{5}{9}$	$\frac{3}{40}$

a term introduced by *Nielsen* [1992] to model the convective effect of vortices generated by the flow over the crest of the ripples moved the sediment concentration profiles in the right direction, but not enough.

[5] More complex time-dependent RANS models for the fluid phase coupled to an SSC equation have been considered, at the cost of forgoing analytical treatment. *Davis et al.* [1997] compared four models with flume experiments of pulsating flows under sheet flow conditions. The effect of turbulence in the SSC equation was modeled with an eddy diffusion ν_s assumed equal or proportional to the eddy viscosity ν_t used in the momentum equation. The models studied differed in how ν_t was calculated. While the models were able to reproduce the mean concentration and velocity profile (with the exception of the simplest one, based on the mixing length concept), with various degrees of success, they failed to reproduce the phase-averaged concentration profiles, and, as a consequence, the contribution to the mean flux due to the oscillating part. The authors attributed the failure to the inability of eddy diffusivity models to capture the convective events that dominate sediment fluxes near the bed during flow reversal. Similar failures have been recently reported by *Dohmen-Janssen et al.* [2001] under sheet flow conditions and by *Thorne et al.* [2002] under ripple favorable conditions. In both cases, fiddling with the parameters of the model improved the agreement between the observed profiles and the measured ones, but no indication was given as to what are the appropriate parameters under general conditions.

[6] Several conjectures exist to explain the failure of the Eulerial-Eulerian RANS/SSC approach: modification of the turbulent properties due to the presence of suspended sediments [*Pan and Banerjee*, 1996; *Boivin et al.*, 2000; *Ribberink and Al-Salem*, 1994; *Dohmen-Janssen et al.*, 2001]; deficiencies in the modeling of the turbulent sediment flux; misrepresentation of the bottom boundary condition for the sediment concentration [*Nielsen et al.*, 2002]; inability of the RANS component to properly model the physics of the flow when turbulent quantities are not in equilibrium or near equilibrium [*Scotti and Piomelli*, 2002].

[7] Let us consider the evolution equation for the SSC

$$\frac{\partial C}{\partial t} + \mathbf{U} \cdot \nabla C = -\nabla \cdot \mathbf{Q}_t,$$

where $\mathbf{U}$ is the Reynolds averaged velocity field and $\mathbf{Q}_t$ is the turbulent sediment flux. The RANS module has to provide a correct description of the velocity field, to properly account for the advective component, and also must provide reasonably accurate values of the turbulent quantities that are used to model the turbulent flux. Thus the RANS model provides the foundation upon which the rest of the modeling effort is built. It is therefore important to determine whether the model is up to the task. RANS models have been tested and calibrated extensively under steady (but not necessarily uniform) conditions. *Guizien et al.* [2003] recently proposed a modification to a RANS model to explicitly take into consideration unsteady effects. Compared to the original, the improved model fared better, but there were still quantitative discrepancies with experimental results. Moreover, the model relied on a somewhat *ad hoc* enhancement of the wall shear when the pressure gradient turns against the flow. It is not clear how the model can be extended to more complex geometries, nor the model takes into account the interaction between unsteady shear and production away from the wall. Therefore more research is needed to asses the validity of RANS models under unsteady conditions and non trivial geometry. We are not aware of any published work in which unsteady RANS were carefully benchmarked under conditions encountered in the ocean. This study is in fact inspired by the work of *Scotti and Piomelli* [2002], who looked at the performance of several RANS models applied to pulsating turbulent boundary layers of the kind encountered in aeronautical applications. While most of the models considered gave a satisfactory description of the mean streamwise velocity as a function of time, discrepancies existed, at least during some part of the cycle, with regard to key quantities such as turbulent kinetic energy, dissipation and Reynolds stress. Further work is needed, however, since the results of *Scotti and Piomelli* [2002] did not address questions that are very important from the point of view of modeling sediment transport (because of the different geometry and parameters). For instance, we cannot say if the phase-averaged vertical component of the velocity over ripples is well reproduced by RANS (since the geometry was flat); when and where the discrepancies with respect to the Reynolds stress occur; how large they are, especially in the separated region. To answer these questions, we follow an approach similar in spirit, but for a model and conditions that are relevant to geophysical processes typical of the coastal environment. The benchmark chosen is a turbulent pulsating flows over ripples. This flow is of particular importance to the ocean community, as it is representative of conditions frequently encountered in the nearshore region. Details of the physics of steady turbulent flows over this particular geometry can be found in *Calhoun and Street* [2001] and *Henn and Sykes* [1999], which used large-eddy simulation (LES) to model the flow. The geometry was set to match the experiments (under steady conditions) of *Hudson et al.* [1996] and the Direct Numerical Simulation (DNS) of *Maaß and Schumann* [1996], which are regarded as standard benchmark. The amplitude to wavelength ratio of the ripples was set to 0.1, large enough to cause separation at the Reynolds numbers considered, and similar to the steepness of ripples observed in lab experiments [*Ribberink and Al-Salem*, 1994; *Sleath and Wallbridge*, 2002]. During the experiments, the frequency and amplitude of the

Table 2. Driving Conditions and Observed Mean Velocities

Case	G_p^o (*m/s*)	$T \equiv 2\pi/\omega$ (*sec*)	u_b (*m/s*), RANS	u_b (*m/s*), LES
0	–	–	0.138	0.135
1	0.13	8.0	0.125	0.116
2	0.26	8.0	0.084	0.082
3	0.13	4.0	0.114	0.108
4	0.26	4.0	0.077	0.082
5	0.13	2.0	0.077	0.091
6	0.26	2.0	0.052	0.085

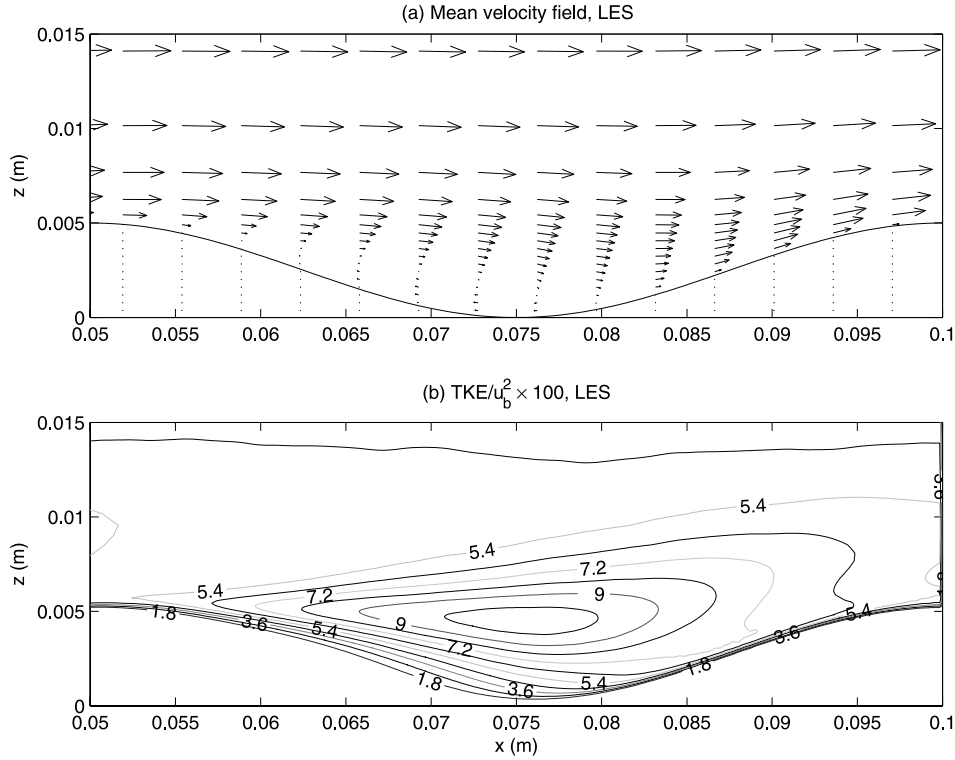

Figure 1. (a) Mean velocity field over ripples under steady conditions. Note the recirculation bubble extending from the crest to about $x/L_x = 0.8$. (b) Mean turbulent kinetic energy. See color version of this figure in the HTML.

oscillation was varied, so that the wavelength, normalized by the orbital amplitude ranged from 0.03 to 0.6, at the lower end of values normally encountered in the field. We are aware that, under these forcing conditions, the ripples that naturally occur are asymmetric [*Yalin*, 1977]. However, we think that it is more important to work under conditions for which good experimental data are available (at least in the steady case), than to consider more realistic ripple topologies. Indeed, the main focus of this paper is to gauge how well RANS models deal with flows characterized by unsteadiness, separation and regions of free shear; the chosen geometry possess all of these properties. The RANS model employed was the $k - \omega$ model of *Wilcox* [1998]. We chose this particular model because it handles regions of adverse pressure gradient better than the more familiar $k - \epsilon$ model [*Guizien et al.*, 2003]. *Fredsœ et al.* [1999] compared its prediction with experiments carried under conditions similar to the one described here. The model compared well with the experiments, but the comparison was limited to thestreamwise horizontal component of the velocity. Here the goal is to verify if the comparison extends to other quantities, such as vertical velocity and turbulent fluctuations.

[8] Ideally, the model should be compared with good experimental data. Unfortunately, we are not aware of any experimental data set that can be used for this purpose (*Fredsœ et al.* [1999] did not report the Reynolds stress nor the turbulent kinetic energy). Instead, we opted to use the results from a well resolved large-eddy simulation (LES), which was validated in the steady case against experimental and numerical (DNS) data. The LES model employed, which does not have tunable parameters, has been widely and successfully used to study steady and unsteady turbulent flows [*Meneveau and Katz*, 2000; *Scotti and Piomelli*, 2001; *Balaras et al.*, 1995; *Piomelli et al.*, 2000; *Balaras et al.*, 2001; *Balaras*, 2004]. The main difference between RANS and LES is that in a LES only the small-scale fluctuations need to be modeled, while in a RANS the Reynolds stress receives contributions from fluctuation at all scales, including the large ones that are directly affected by the forcing and boundary conditions. Hence LES is widely regarded to have a more universal character [*Lesieur and Metais*, 1996].

[9] The rest of the paper is organized as follows: In section 2 we present the details of the models employed and compare them with available experimental data in the steady case; next, we consider the unsteady case, comparing the phase averaged prediction of RANS and LES with regard to streamwise and vertical velocity, turbulent kinetic energy and Reynolds Stress; finally, we discuss the results in the last section.

2. Problem Formulation and Validation

2.1. Wilcox ($k - \omega$) Model

[10] The model solves the two-dimension phase-averaged Navier-Stokes equations

$$\frac{\partial U_i}{\partial t} + U_j \frac{\partial U_i}{\partial x_j} = -\frac{1}{\rho}\frac{\partial P}{\partial x_i} + \frac{\partial}{\partial x_j}\left(2\nu S_{ij} - R_{ij}\right) + G_p, \qquad \frac{\partial U_i}{\partial x_i} = 0, \tag{1}$$

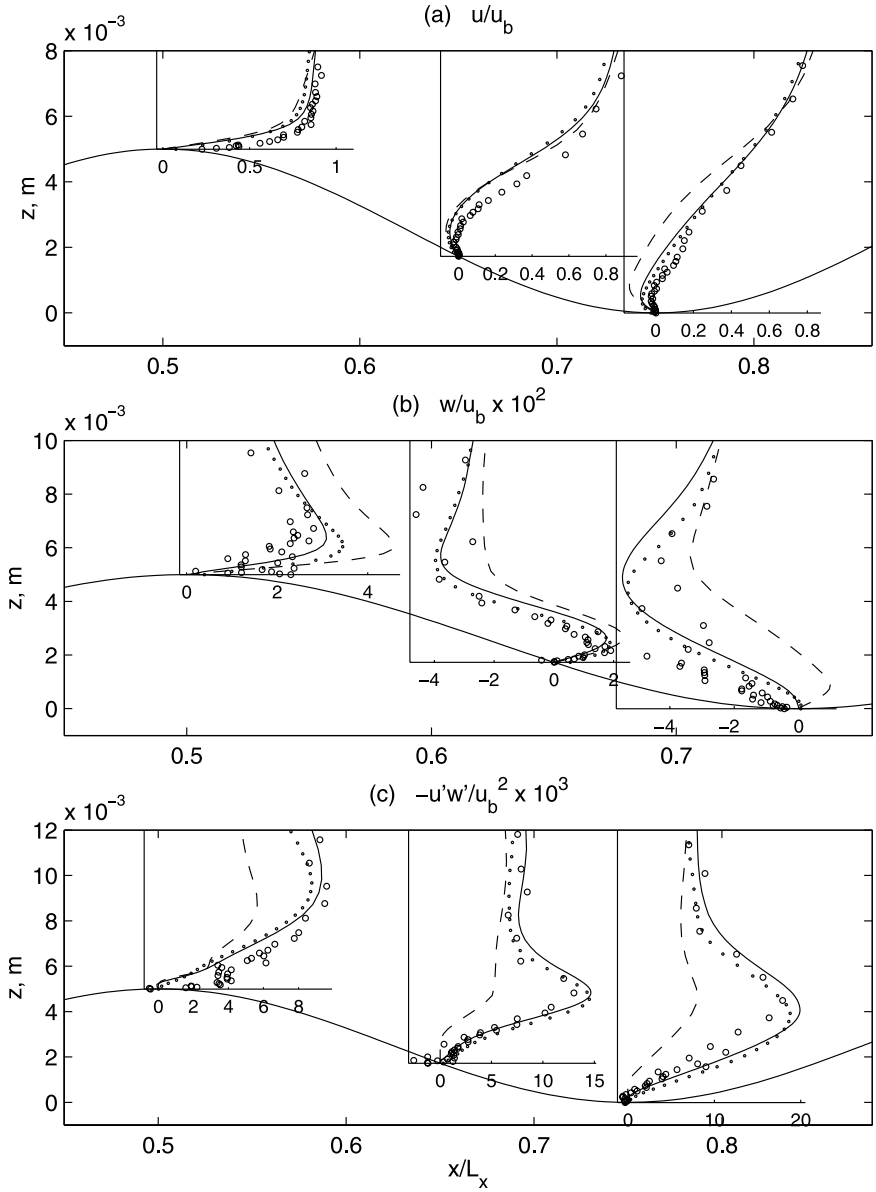

Figure 2. Comparison between the measurements of *Hudson et al.* [1996] (large circles), DNS of *Maaß and Schumann* [1996] (small circles), LES (solid line), and RANS (dashed line) at three different locations along the ripple surface: (a) mean streamwise component, (b) mean vertical component, and (c) Reynolds stress. The flow is driven by a steady pressure gradient.

where U_i is the phase-averaged velocity vector, S_{ij} is the phase-averaged rate of strain tensor, G_p the external pressure gradient divided by the fluid density and R_{ij} the Reynolds stress tensor, which, under the Boussinesq approximation, is written as

$$-R_{ij} = 2\nu_t S_{ij} - \frac{2}{3}k\delta_{ij}. \tag{2}$$

[11] In order to close the system of equations the model writes the eddy viscosity ν_t as the ratio of the turbulent kinetic energy k and the dissipation rate timescale ω, which obey the following transport equations

$$\frac{\partial k}{\partial t} + U_j\frac{\partial k}{\partial x_j} = \frac{\partial}{\partial x_j}\left[(\nu + \sigma^*\nu_t)\frac{\partial k}{\partial x_j}\right] - \overline{u_i u_j}\frac{\partial U_i}{\partial x_j} - \beta^* k\omega, \tag{3}$$

$$\frac{\partial \omega}{\partial t} + U_j\frac{\partial \omega}{\partial x_j} = \frac{\partial}{\partial x_j}\left[(\nu + \sigma\nu_t)\frac{\partial \omega}{\partial x_j}\right] - \gamma\frac{\omega}{k}\left(\overline{u_i u_j}\frac{\partial U_i}{\partial x_j}\right) - \beta k\omega^2. \tag{4}$$

[12] The equations are solved in two-dimension ($x - z$) by a finite volume method on an orthogonal curvilinear grid. The physical domain is a half channel with mean height, $H/2$ = 0.025 m and length, L_x = 0.1 m. The domain has two sinusoidal ripples on the bottom with height from crest to trough h_r = 0.005 m, and wavelength λ_r = 0.05 m, so that h_r/λ_r = 0.1. The domain is uniformly discretized with 120 and 60 points in the streamwise and vertical direction. The bottom boundary conditions are no-slip for the velocities and k = 0. For ω it is given as a function of the friction velocity and Nikuradse's roughness. On the lateral boundaries periodic boundary conditions are applied. Table 1 lists the value of the

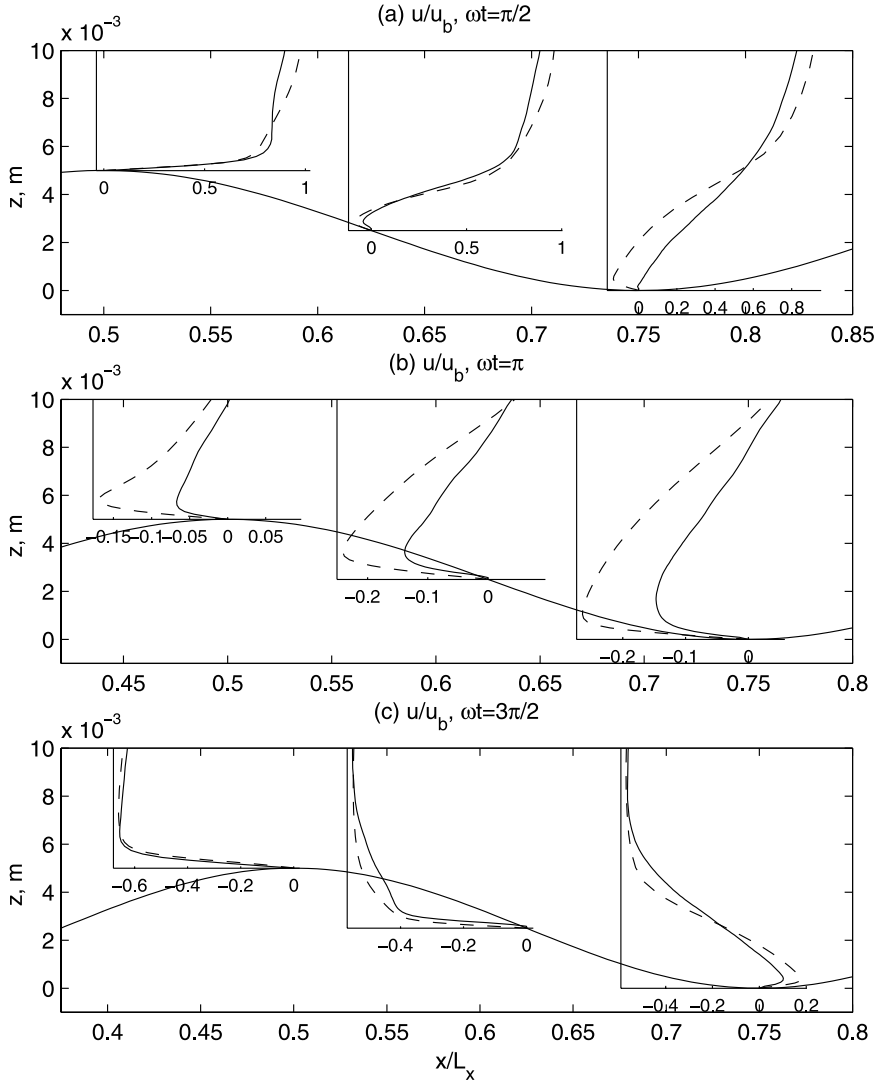

Figure 3. Horizontal velocities(u) at different phases, case 4: (a) $\omega t = \pi/2$, (b) $\omega t = \pi$, and (c) $\omega t = 3\pi/2$. Solid line is LES and dashed line is RANS; $u_b = \max U$ at $\omega t = \pi$.

constant used in the model. Details of the models can be found in Andersen's Ph.D. thesis [*Andersen*, 1999].

2.2. Large-Eddy Simulation

[13] The unsteady velocity and pressure fields are obtained by solving the filtered Navier-Stokes equations

$$\frac{\partial \tilde{u}_i}{\partial t} + \frac{\partial}{\partial x_j}\left(\tilde{u}_i \tilde{u}_j\right) = -\frac{\partial \tilde{P}}{\partial x_i} + \nu \frac{\partial^2 \tilde{u}_i}{\partial x_j \partial x_j} - \frac{\partial \tau_{ij}}{\partial x_j} + G_p, \frac{\partial \tilde{u}_i}{\partial x_i} = 0, \tau_{ij} = \left(\widetilde{u_i u_j} - \tilde{u}_i \tilde{u}_j\right), \quad (5)$$

where the tilde notation is used to indicate filtered variables

$$\tilde{f}(\mathbf{x}) = \int_D G_\Delta(\mathbf{x} - \mathbf{y}) f(\mathbf{y}) d\mathbf{y}$$

and G_Δ is the kernel associated to the top hat filter. The subgrid-scale stress τ_{ij} is modeled using the Lagrangian dynamic eddy viscosity model of *Meneveau et al.* [1996].

[14] The equations are solved using an Adam-Bashfort fractional step method with both advective and diffusive terms treated explicitly. The streamwise L_x and spanwise length L_y of the channel are both set to 0.1 m and the total height $H = 0.05$ m. The ripples are uniform in the spanwise direction and are identical to the one considered in the RANS model. The three-dimensional computational grid is equally spaced in each horizontal direction using 290 points in the streamwise and 66 points in the spanwise direction. In the vertical, equally spaced grid points are used from the bottom to the crest of the ripples, and a hypertangential grid generator is used above the crest for a total of 130 grid points. Periodic boundary conditions are applied in the horizontal direction, and no-slip condition on the upper and lower boundaries, using the immersed boundary technique on the latter [*Mohd-Yusof*, 1997; *Fadlun et al.*, 2000; *Balaras*, 2004]. The flow is driven by the external pressure gradient ρG_p.

2.3. Simulation Parameters and Data Reduction

[15] In all the experiments, $\nu = 10^{-6}$ m^2/s, and the external pressure gradient is given by

$$G_p = G_p^s + G_p^o \omega \cos(\omega t).$$

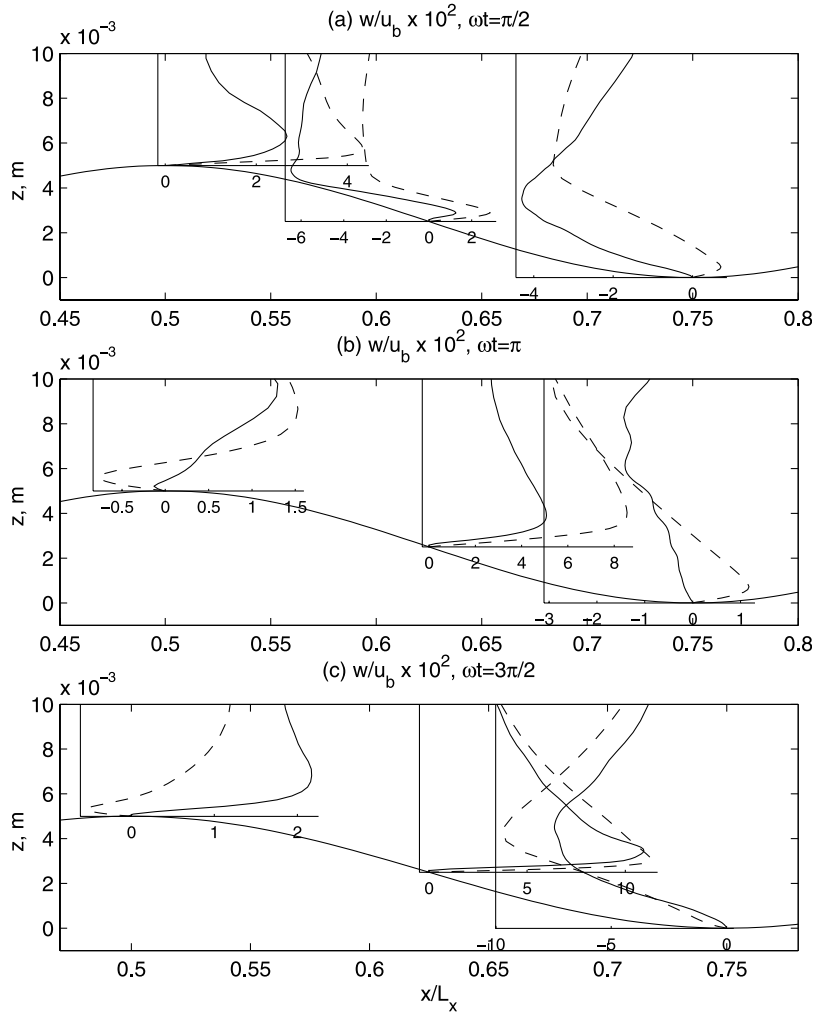

Figure 4. Vertical velocities (w) at different phases, case 4: (a) $\omega t = \pi/2$, (b) $\omega t = \pi$, and (c) $\omega t = 3\pi/2$. Solid line is LES and dashed line is RANS; $u_b = \max U$ at $\omega t = \pi$.

We consider two sets of experiments, steady and pulsating. In the steady case, we set $\omega = 0$ and run the models adjusting G_p^s to obtain a statistically steady flow with a mean streamwise velocity equal to 13.5 cm/s. The purpose of the exercise is twofold: determine the value of G_p^s needed to give achieve the Reynolds number matching the experiments of *Hudson et al.* [1996] and the DNS data of *Maaß and Schumann* [1996] for validation purposes (this value is than used in the pulsating experiments); to provide a suitable initial condition for the pulsating experiments. In the pulsating case, we consider six sets of driving conditions, with periods varying from 2 to 8 seconds, and G_p^o ranging from 0.13 m/s to 0.26 m/s. G_p^s is kept constant at the value determined above (Table 1). Table 2 lists the parameters used in each case. In each experiments, the flow is simulated for 20 cycles, and averages are performed over the last 10.

[16] In a pulsating turbulent flow, driven at a specific frequency ω, any fluctuating quantity $f(\mathbf{x}, t)$ can be written as

$$f(\mathbf{x},t) = \langle f \rangle_p(x,z,t) + f'(\mathbf{x},t) = F + f',$$

where $\langle\ \rangle_p$ denotes the phase averaging procedure, and f' is the turbulent remainder. Moreover, the time dependence of the phase-averaged component can be analyzed in terms of harmonic analysis

$$F \equiv \langle f \rangle_p(x,z,t) = F_0(x,z) + \sum_{n=1}^{\infty} F_n(x,z)\sin(n\omega t + \alpha_n(x,z)).$$

In analogy with the theory of electrical circuits, we call F_0 the DC part, and F_1 the AC part.

2.4. Steady Turbulent Boundary Layer Over Ripples

[17] Even though a detailed discussion of the physical properties of a turbulent boundary layer over sinusoidal ripples is beyond the scope of this paper, it useful to give a brief outline of the main features observed in the steady case. *Hudson et al.* [1996] divide the flow into an outer region ($z > 0.25\ H$), which is weakly affected by the presence of the ripples, and an inner region where the flow is significantly modified. The inner region can be further subdivided into three areas: An accelerating boundary layer along the upslope side of the ripple, driven by a strong favorable pressure gradient; a recirculation bubble extending from about 0.2λ downstream of the crest to a point downstream of the trough; and a shear layer capping the

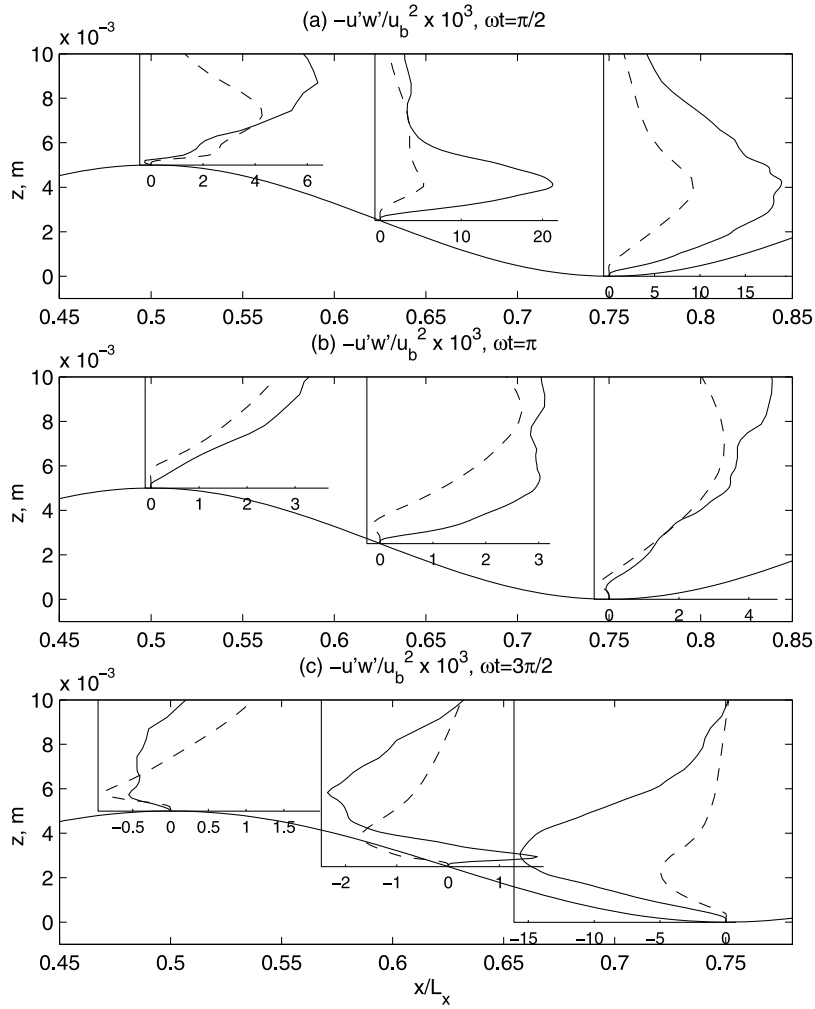

Figure 5. Reynolds stresses ($-\overline{u'w'}$) at different phases, case 4: (a) $\omega t = \pi/2$, (b) $\omega t = \pi$, and (c) $\omega t = 3\pi/2$. Solid line is LES and dashed line is RANS; $u_b = \max U$ at $\omega t = \pi$.

recirculation bubble (Figure 1a). The shear layer is where most of the turbulent kinetic energy (TKE) is found, while little TKE exists along the upslope because of the stabilizing effect of the favorable pressure gradient (Figure 1b). Despite the simple geometry, the steady flow contains several elements that are difficult to model: separation, reattachment, unbounded shear layers and accelerating layers. The addition of unsteadiness adds another layer of complexity.

2.5. Validation

[18] Here and in the rest of the paper, we focus on the dynamics in the lee of the ripple (defined relative to the mean flow). The rationale is that several studies [*Zedler and Street*, 2001, 2002; *Chang and Scotti*, 2003] suggest that the lee of the ripple is a particularly critical area for sediment ejection into the outer flow. Also, at least for the flows characterized by large oscillations of the velocity, the lee becomes the stoss side, at least during part of the cycle.

[19] Under steady conditions, RANS and LES give essentially the same answer with regard to the mean streamwise velocity, the exception being at the trough, where RANS predicts a larger backward flow near the surface of the ripple (Figure 2a). The situation changes when we consider the mean vertical velocity. Good agreement is found between experiments, LES and DNS. However, RANS overpredicts the vertical velocity at the crest and gives a qualitatively different picture at the trough. The most likely explanation is that the reattachment point in RANS is located further downstream than observed (Figure 2b). With regard to the Reynolds stress, the situation is similar. We see again an excellent agreement between experiments, LES and DNS. RANS, on the other hand, consistently underestimates the peak in stress found at the edge of the shear layer capping the recirculation bubble in the lee of the ripple (Figure 2c). Hence we tentatively conclude that LES can be considered a valid surrogate to "real" data.

[20] The question remains whether this statement remains valid when LES is applied to unsteady flows. The question of applicability of LES to unsteady flows was considered in *Scotti and Piomelli* [2001], where it was shown that LES, employing the same dynamic eddy viscosity model used here, compared very well with existing experimental and numerical studies of pulsating boundary layers over flat surfaces, even to the point of capturing subtle effects related to the modulation of near-wall structures. Thus nothing in

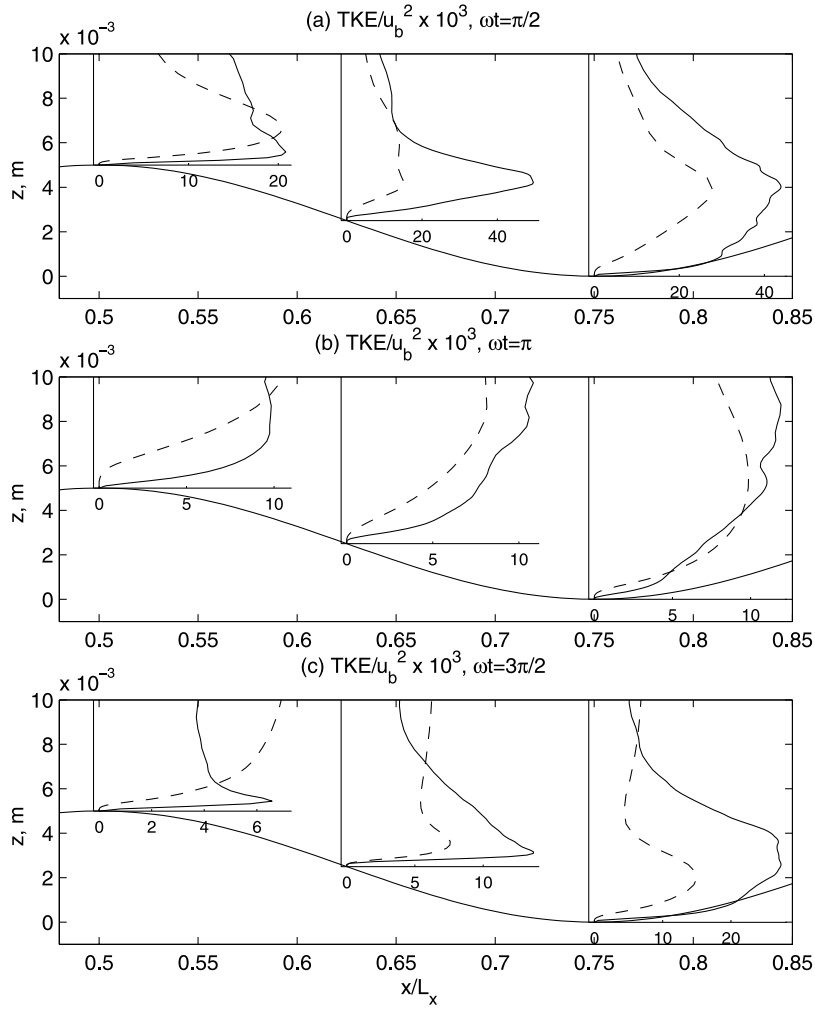

Figure 6. Turbulent kinetic energy (*TKE*) at different phases, case 4: (a) $\omega t = \pi/2$, (b) $\omega t = \pi$, and (c) $\omega t = 3\pi/2$. Solid line is LES and dashed line is RANS; $u_b = \max U$ at $\omega t = \pi$.

the available literature suggests that LES might fail in the case at hand.

3. Pulsating Flows

[21] With the oscillating component of the pressure gradient turned on, the first obvious effect is a decrease of the mean velocity. Since the mean component of the external pressure gradient is kept constant, the effect of the oscillations is to increase the drag exerted by the ripples over the flow. Both RANS and LES exhibit this phenomenon with similar results.

[22] To consider the changes more in detail we analyze in depth case 4, and then consider the effects of changing frequency and amplitude. We compare the results at three phases of the cycle, namely during maximum forward flow ($\omega t = \pi/2$), maximum deceleration ($\omega t = \pi$) and during maximum reverse flow ($\omega t = 3\pi/2$) and at three locations along the ripple (crest, midslope and trough). With regard to the streamwise component of the velocity, the agreement between RANS and LES is good during times of maximum forward or reverse flow, with the largest discrepancy found in the trough. The situation is different during the decelerating phase, where it appears that flow reversal in the boundary layer occurs earlier in RANS than in LES (Figure 3). The comparison is much worse if we consider the vertical velocities. The only case in which LES and RANS agree well is on the midslope location during maximum backward flow, that is in a region of strong downstream acceleration. Large quantitative (crest at $\omega t = \pi/2$, midslope at $\omega t = \pi$ and trough at $\omega t = 3\pi/2$) and qualitative differences (elsewhere) dominate the flow (Figure 4). In the midslope region at $\omega t = \pi/2$ and in the trough, the difference is a likely indicator that RANS and LES give different predictions with regard to the strength and size of the recirculation area in the lee of the ripple.

[23] The major qualitative difference in the phase-averaged Reynolds stress $-\langle u'w' \rangle_p$ is found along the upslope section during maximum backward flow, which might be due to the presence of strong and well organized vortices [*Henn and Sykes*, 1999; *Calhoun and Street*, 2001; *Chang and Scotti*, 2003] which the LES captures but are not accounted for by RANS (Figure 5). Large qualitative differences exists across the shear layer that forms in the lee of the ripple, where RANS severely underpredicts the magni-

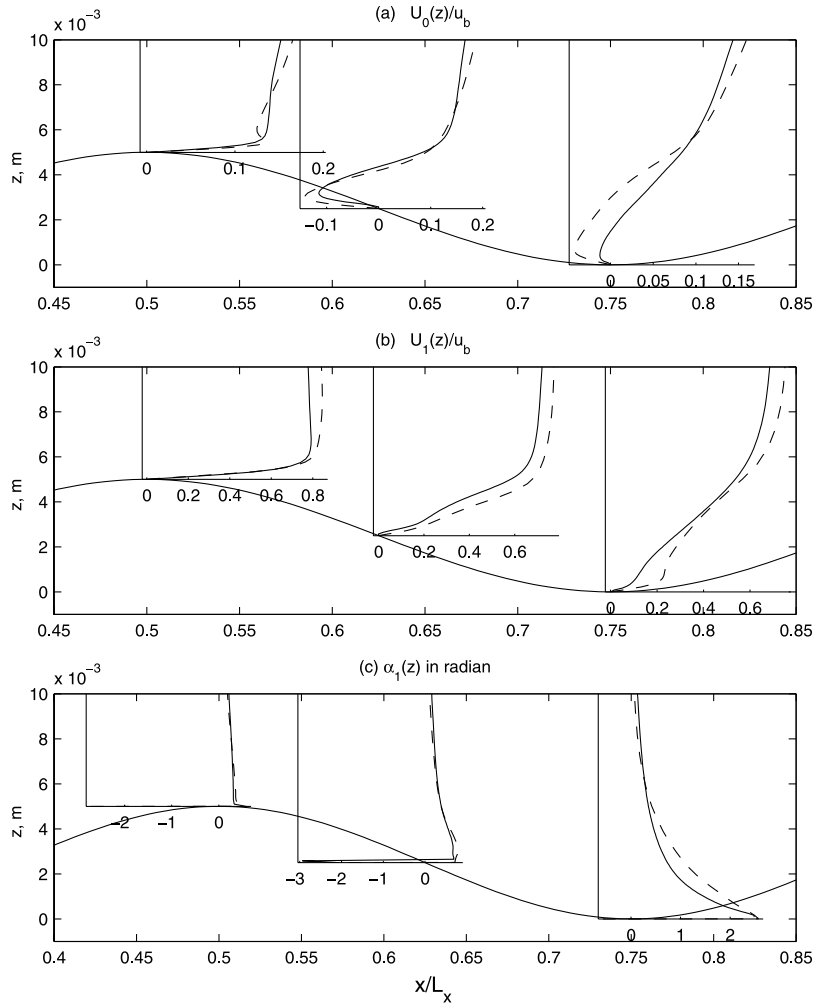

Figure 7. Period average (U_0), amplitude (U_1), and phase (α_1) of the component of the phase-averaged horizontal velocity oscillating at the driving frequency, case 4: (a) U_0, (b) U_1, (c) α_1^U. Solid line is LES and dashed line is RANS; $u_b = \max U$ at $\omega t = \pi$.

tude of the Reynolds stress relative to LES. A similar trend is found in the steady case. Also, in the vicinity of the boundary, RANS predicts a region of uniform (and small) values of the stress. On the other hand, during flow reversal the agreement is quite good. The profiles of turbulent kinetic energy k show a similar pattern. RANS underestimates k across the shear layer and along the upslope during backward flow (Figure 6).

[24] So far we have considered instantaneous snapshots of the fields at different times. A more synoptic way to look at the problem is to use harmonic analysis.

[25] Not surprisingly, LES and RANS gives similar profiles for the DC component and the amplitude and phase of the AC component of the streamwise velocity. The largest variation is found in the trough, likely due to differences in the location of the reattachment point (Figure 7). For the vertical velocity, the DC component shows a pattern similar to the one observed in the steady case. RANS overestimates the velocity near the crest, and there is a small qualitative difference at the trough (Figure 8a). The largest variations are found in the amplitude and phase of the AC component, where RANS predicts oscillations two to three times larger than LES, with a significant phase difference (Figures 8b and 8c).

[26] The largest differences in the estimate of the horizontal velocity between LES and RANS are found around $\omega t = \pi$, at the peak of the decelerating phase. The same is true at higher driving frequencies (case 6) as well as at lower frequencies (case 2), as can be seen in Figure 9. Despite the difference in magnitude, LES and RANS predicts the same trend of increasing backward flow with decreasing frequency. The same cannot be said of the predicted Reynolds stress. In fact, LES shows an increase in Reynolds stress as the period decreases, while RANS shows the opposite trend (Figure 10). A possible explanation of this effect is that as the driving frequency increases, turbulence in the flow departs more and more from the state of equilibrium under which the RANS model was originally derived.

[27] At the end of the accelerating phase ($\omega t = \pi/2$), the Reynolds stress predicted by RANS and LES agree quite well in case 2, but otherwise RANS severely underestimates the peak in Reynolds stress in the shear layer, becoming increasing worse at higher frequencies (Figures 11 and 12).

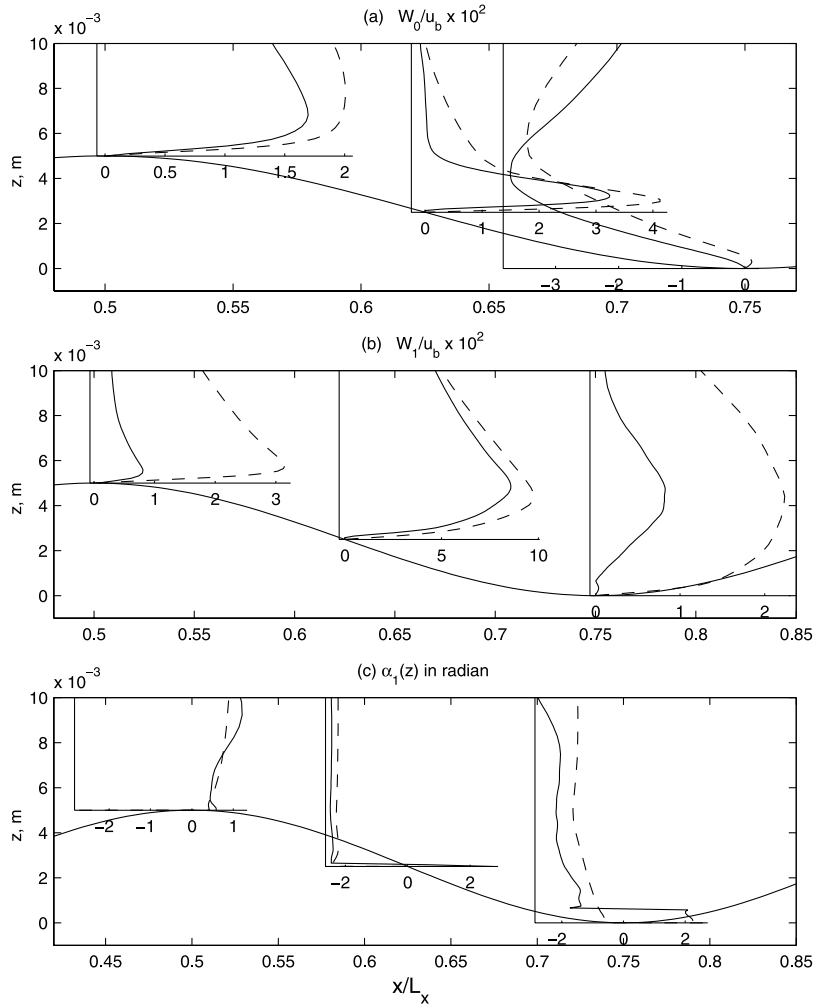

Figure 8. Time-averaged and oscillating components of the vertical velocity, case 4: (a) W_0, (b) W_1, and (c) α_1^w. Solid line is LES and dashed line is RANS; $u_b = \max U$ at $\omega t = \pi$.

[28] We finally consider the magnitude of the bottom stress as a function of time and position along the surface of the ripple. The agreement is overall quite good, especially over the crest. Along the downslope and in the trough RANS tends to overestimate the stress, especially during flow reversal (Figure 13).

4. Discussion and Summary

[29] Unsteady turbulent flows over ripples are difficult to model because they are characterized by the simultaneous presence of flow separation, regions of unbounded shear and unsteadiness. From this point of view, it is surprising that a RANS model can actually capture some of the properties with a good degree of accuracy. The data presented in this paper confirm earlier finding [*Scotti and Piomelli*, 2002] that RANS models give a correct description of the streamwise velocity profile. It follows that quantities derived from $U(x, z)$ are also well reproduced, especially if they are spatially averaged, such as the wave-current friction coefficient. However, the applicability to problems of sediment transport at the ripple-scale level require the correct modeling of the entire turbulent flow. Under this respect, and for the specific case of pulsating flow, the RANS model considered is deficient in two ways. It severely underestimates the Reynolds stress in the shear layer that forms in the lee of the ripple, and overestimates the amplitude of the oscillations in the vertical velocity. The two problems are likely to be related and also offer an explanation as to why the horizontal momentum profiles agree well with the LES, despite the low value of the Reynolds stress. Indeed, the total momentum flux experienced by the flow is the sum of the Reynolds stress $\langle u'w' \rangle$ and the stress due to the macroscopic motion of fluid particles induced by the ripples (which is absent if the flow is over a flat surface). The averaged value over a cycle of the latter term

$$\frac{1}{T}\int_0^T UW\,dt = U_0 W_0 + \frac{U_1 W_1}{2}\cos\left(\alpha_1^u - \alpha_1^w\right) + \cdots$$

contains a contribution from the oscillating terms. We hypothesize that the larger values of W_1 observed in the RANS balance the lower values of $\langle u'w' \rangle$, so that the net downward momentum flux is preserved. Can a similar

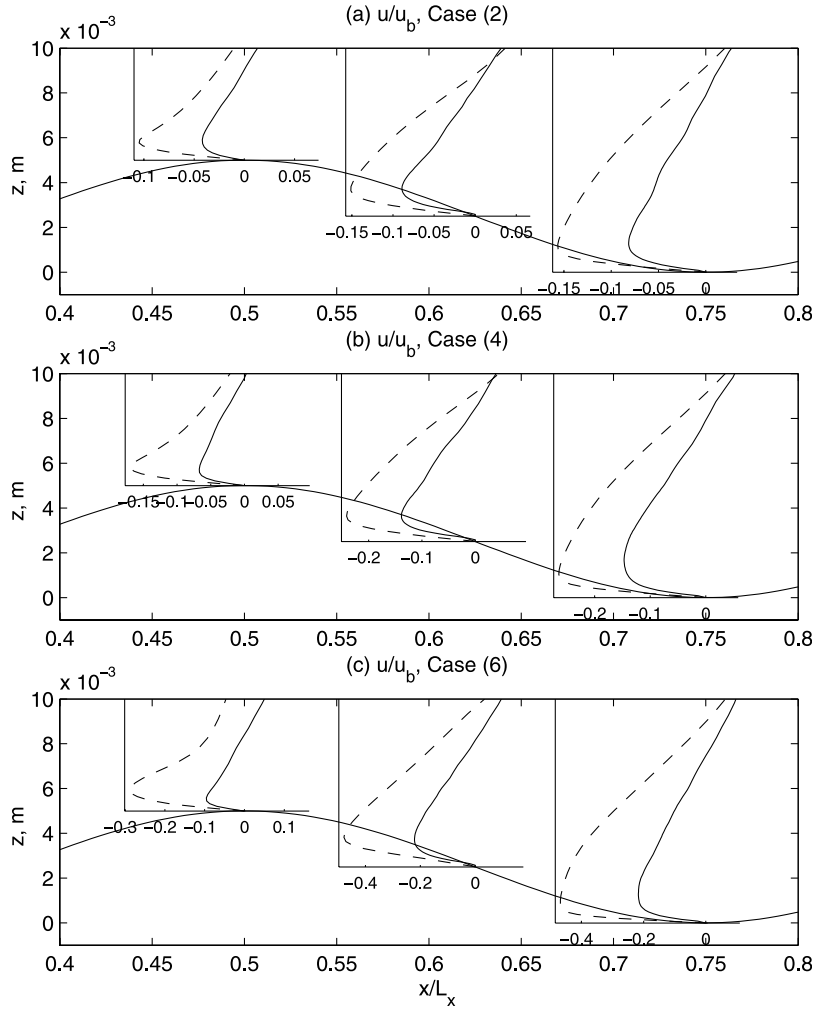

Figure 9. Horizontal velocities (u) with different oscillating periods, cases 2, 4, and 6 at $\omega t = \pi$. Solid line is LES and dashed line is RANS; $u_b = \max U$ at $\omega t = \pi$.

compensation take place at the level of sediment fluxes? On the basis of the available literature, the answer is a probable no. Low values of the Reynolds stress translate to low values of the estimated eddy diffusivity (assuming that the turbulent Schmidt number is O(1)). The concentration profile is much steeper over ripples than the horizontal momentum distribution, so that in the total sediment flux

$$(W - w_s)C + \nu_t \frac{\partial C}{\partial z}$$

the contribution of the last term should dominate. Moreover, we know from numerical experiments that sediments are ejected into the flow above the ripples primarily by the instabilities in the shear layer [*Chang and Scotti*, 2003], which remove sediments from the cloud that forms in the ripples, precisely where the largest discrepancy in the prediction of the Reynolds stress occurs between RANS and LES. The latter problem exists under steady conditions as well, but worsen with decreasing forcing period. While the present work deals with a somewhat unrealistic ripple geometry for the type of forcing considered (i.e., symmetric ripples), there is no reason to doubt that the main result will carry over to more realistic conditions, such as asymmetric ripples.

[30] A legitimate question is whether improved RANS models can be developed to ameliorate the situation. Though it is not wise to predict the future, we must observe that RANS is a mature technique, and it is difficult to break new ground. In addition to that, RANS has always suffered from the need to tune the (usually many) parameters of the model to the particular case under consideration. DNS, and the new generation of LES models (such as the one employed for this study) do not suffer from this requirement. A further reason to move away from RANS to model the physics of small-scale sediment transport is the growing evidence about the role played by coherent structures in the entrainment of sediments in the vicinity of the boundary [*Sumer and Oğuz*, 1978; *Sumer and Deigaard*, 1981; *Sumer et al.*, 1996; *Zedler and Street*, 2001; *Vittori*, 2003]. Fortunately, the tremendous increase in computational power that happened in the last decade has made DNS and LES much more affordable [*Piomelli et al.*, 2001]. We hope that this article will contribute in ushering LES into the mainstream of sediment transport studies.

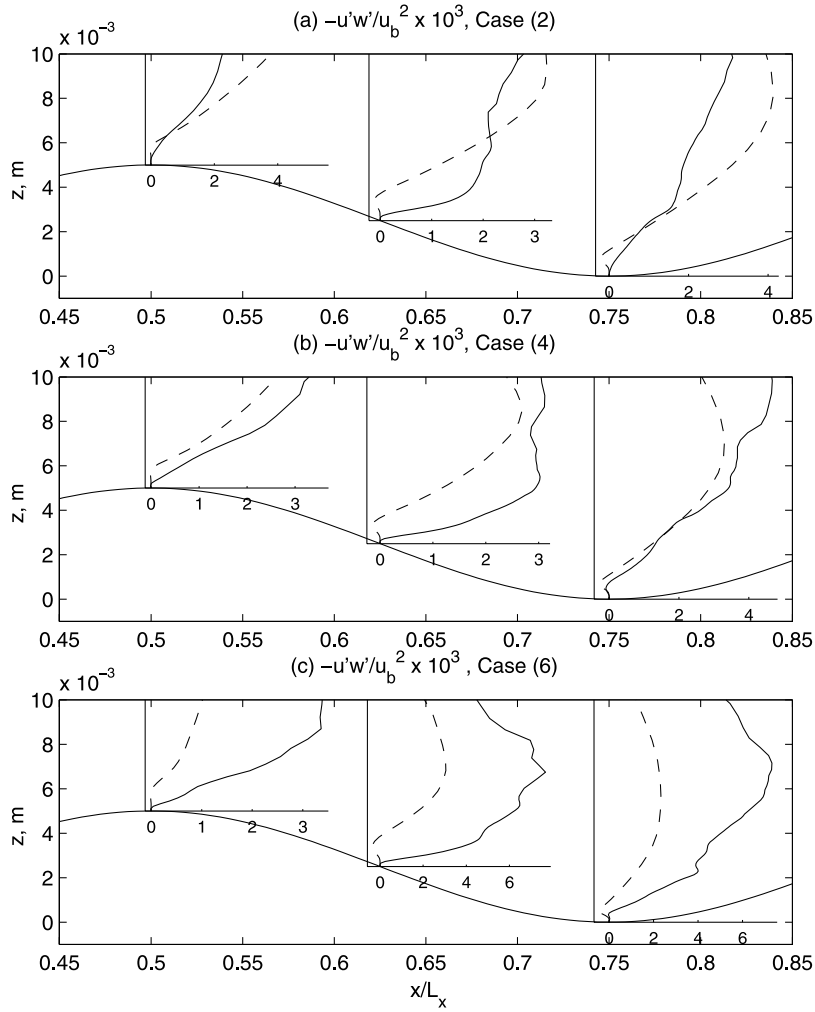

Figure 10. Reynolds stresses ($-\overline{u'w'}$) with different oscillating periods, cases 2, 4, and 6 at $\omega t = \pi$. Solid line is LES and dashed line is RANS; $u_b = \max U$ at $\omega t = \pi$.

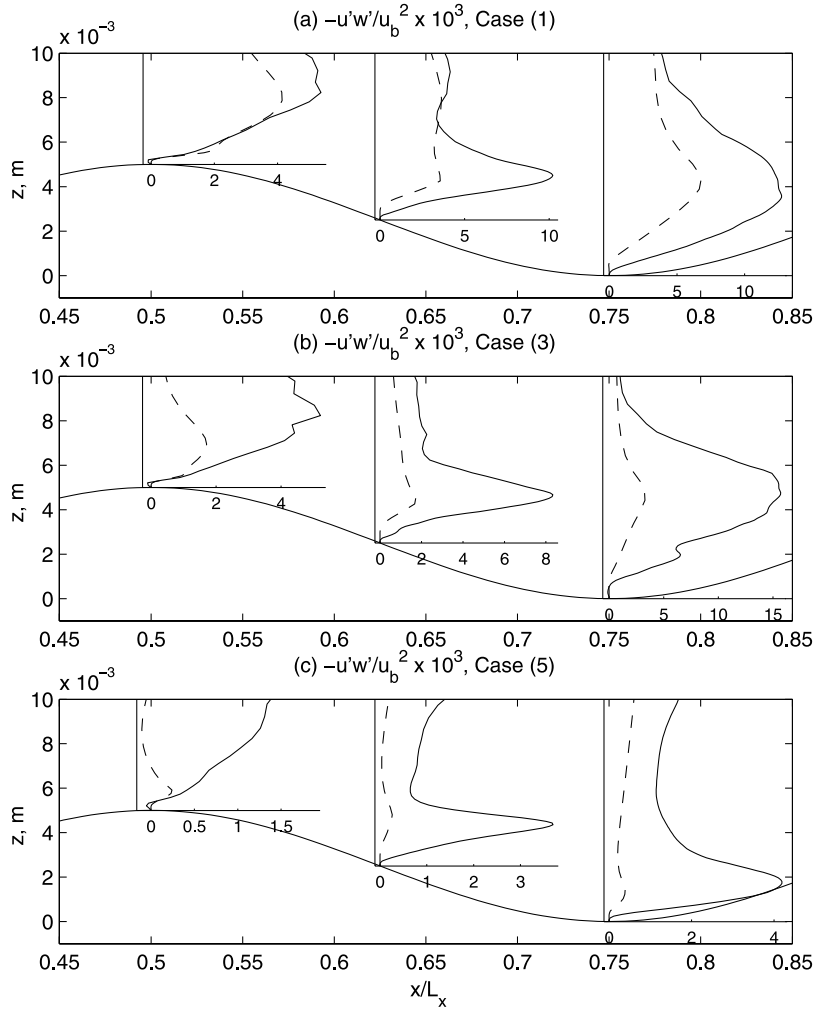

Figure 11. Reynolds stresses ($-\overline{u'w'}$) with $G_p^o = 0.13$ m/s at $\omega t = \pi/2$, cases 1, 3, and 5. Solid line is LES and dashed line is RANS; $u_b = \max U$ at $\omega t = \pi$.

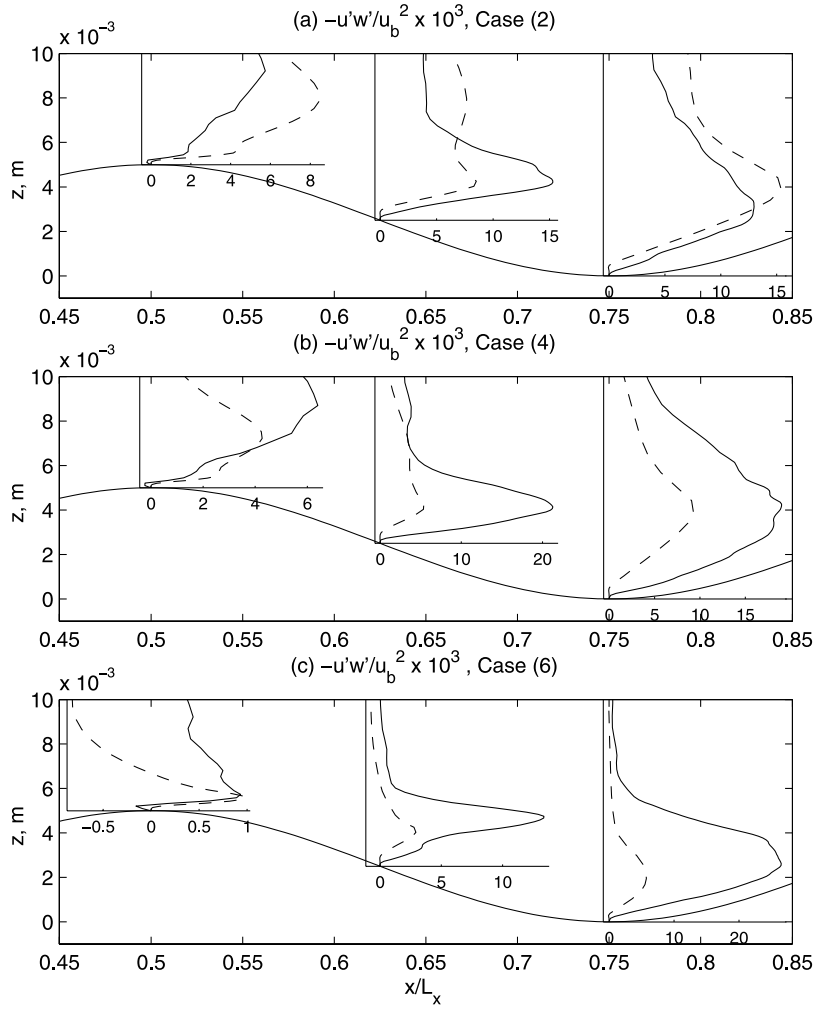

Figure 12. Reynolds stresses ($-\overline{u'w'}$) with $G_p^o = 0.26$ m/s at $\omega t = \pi/2$, cases 2, 4, and 6. Solid line is LES and dashed line is RANS.

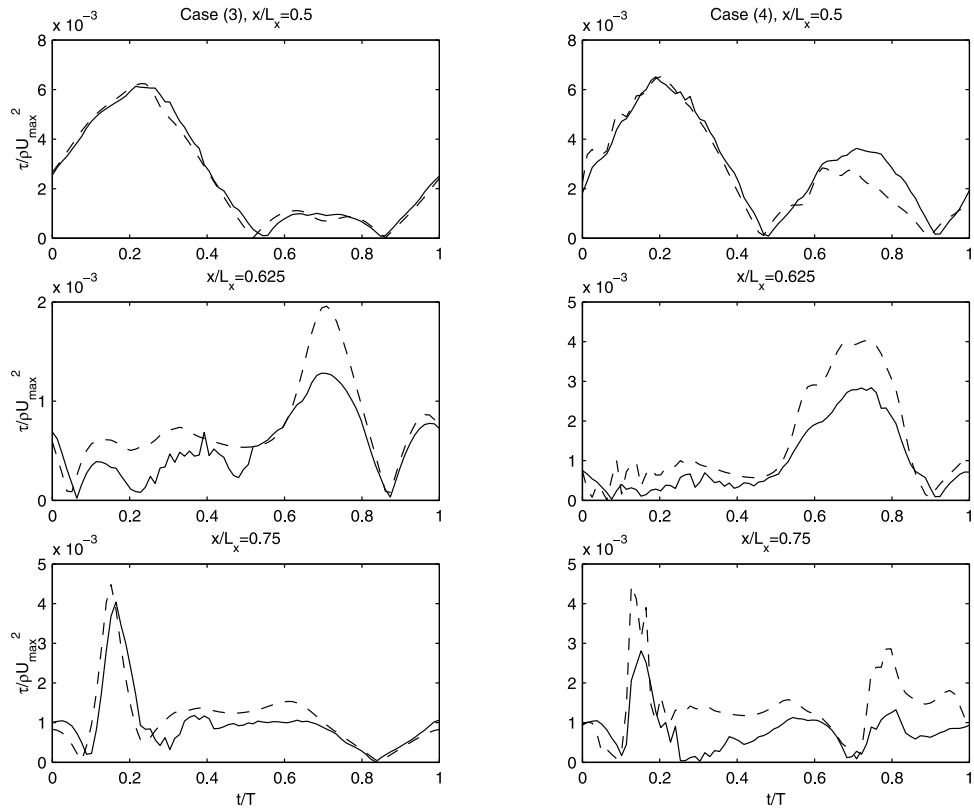

Figure 13. Bottom shear stresses over one wave period, cases 3 and 4. Solid line is LES and dashed line is RANS.

[31] **Acknowledgments.** The authors would like to thank Dr. K. H. Andersen for providing us with his implementation of the $k - \omega$ model (DUNE) and Dr. E. Balaras and Dr. D. Hanes for useful discussions. We also wish to thank two anonymous referees for their suggestion to improve the manuscript. This work has been supported by NSF grant OCE–9910883. Numerical calculations were performed on hardware partially funded by NSF grant DMS–0116625. The collaboration of the ATN personnel at UNC is gratefully acknowledged.

References

Andersen, K. H. (1999), The dynamics of ripples beneath surface waves, Ph.D. thesis, Tech. Univ. of Denmark, Lyngby.

Balaras, E. (2004), Modeling complex boundaries using an external force field on fixed Cartesian grids in large-eddy simulation, *Comput. Fluids*, *33*, 375–404.

Balaras, E., C. Benocci, and U. Piomelli (1995), Finite difference computations of high Reynolds number flows using the dynamic subgrid-scale model, *Theor. Comput. Fluid Dyn.*, *7*, 207–216.

Balaras, E., U. Piomelli, and J. M. Wallace (2001), Self-similar states in turbulent mixing layers, *J. Fluid Mech.*, *446*, 1–24.

Boivin, M., O. Simonin, and K. Squires (2000), On the prediction of gas-solid flows with two-way coupling using large eddy simulation, *Phys. Fluids*, *12*(8), 2080–2090.

Calhoun, R. J., and R. L. Street (2001), Turbulent flow over a wavy surface: Neutral case, *J. Geophys. Res.*, *106*, 9277–9294.

Chang, Y., and A. Scotti (2003), A numerical study of entrainment and suspension of sediments into a turbulent flow over ripples, *J. Turbulence*, *4*, 019.

Davis, A., J. Ribberink, A. Temperville, and J. Zyserman (1997), Comparisons between sediment transport models and observations made in wave and current flows above plane beds, *Coastal Eng.*, *31*, 163–198.

Dohmen-Janssen, C., W. Hassan, and J. Ribberink (2001), Mobile-bed effects in oscillatory sheet flow, *J. Geophys. Res.*, *106*, 27,103–27,115.

Fadlun, E. A., R. Verzicco, P. Orlandi, and J. Mohd-Yusof (2000), Combined immersed boundary finite difference methods for three-dimensional complex flow simulations, *J. Comput. Phys.*, *161*, 35–60.

Fredsœ, J., K. H. Andersen, and B. M. Sumer (1999), Wave plus current over a ripple-covered bed, *Coastal Eng.*, *38*, 177–221.

Gotoh, H., T. Tsujimoto, and H. Nakagawa (1993), Numerical model of granular material for the dynamics of bed-load layer, in *Proc. 25th Congr. Int. Assoc. Hydraul. Res.*, vol. B-1–4, pp. 33–40.

Gotoh, H., T. Tsujimoto, and H. Nakagawa (1994), Numerical model of interphase momentum transfer and interparticle collision in bed-load layer, in *Proc. 9th Congr. Asia Pac. Div. Int. Assoc. Hydraul. Res.*, edited by H.-F. Cheong et al., pp. 565–572.

Gotoh, H., T. Tsujimoto, and H. Nakagawa (1995), Refined psi-cell model for interphase and interparticle momentum transfer in bed-load layer, *J. Hydrosci. Hydraul. Eng.*, *13*, 13–24.

Grant, W. D., and O. S. Madsen (1979), Combined wave and current interaction with rough bottom, *J. Geophys. Res.*, *84*, 1797–1808.

Guizien, K., M. Dohmen-Janssen, and G. Vittori (2003), 1DV bottom boundary layer modeling under combined wave and current: Turbulent separation and phase lag effects, *J. Geophys. Res.*, *108*(C1), 3016, doi:10.1029/2001JC001292.

Henn, D., and R. Sykes (1999), Large-eddy simulation of flow over wavy surfaces, *J. Fluid Mech.*, *383*, 75–112.

Hudson, J. D., L. Dykhno, and T. J. Hanratty (1996), Turbulence production in flow over a wavy wall, *Exp. Fluids*, *20*, 257–265.

Lee, T., and D. Hanes (1996), Comparison of field observations of the vertical distribution of suspended sand and its prediction by models, *J. Geophys. Res.*, *101*, 3561–3572.

Lesieur, M., and O. Metais (1996), New trends in large-eddy simulatios of turbulence, *Annu. Rev. Fluid Mech.*, *28*, 1–32.

Maaß, C., and U. Schumann (1996), Direct numerical simulation of separated turbulent flow over a wavy boundary, in *Flow Simulation With High Performance Computers II: DFG Priority Research Programme Results 1993–1995*, *Notes Numer. Fluid Mech.*, vol. 52, edited by E. H. Hirschel, pp. 227–241, Braunschweig, Wiesbaden, Germany.

Meneveau, C., and J. Katz (2000), Scale invariance and turbulence models for large-eddy simulation, *Annu. Rev. Fluid Mech.*, *32*, 1–32.

Meneveau, C., T. S. Lund, and W. H. Cabot (1996), A Lagrangian dynamic subgrid-scale model of turbulence, *J. Fluid Mech.*, *319*, 353–385.

Mohd-Yusof, J. (1997), Combined immersed boundaries/b-splines methods for simulations of flows in complex geometries, in *CTR Annual Research Briefs*, NASA Ames/Stanford Univ., Stanford, Calif.

Nielsen, P. (1992), *Coastal Bottom Boundary Layers and Sediment Transport*, *Adv. Ser. Ocean Eng.*, vol. 4, World Sci., River Edge, N. J.

Nielsen, P., K. van der Wal, and L. Gillan (2002), Vertical fluxes of sediment in oscillatory sheet flow, *Coastal Eng.*, *45*, 61–68.

Pan, Y., and S. Banerjee (1996), Numerical simulation of particle interactions with wall turbulence, *Phys. Fluids*, *8*(10), 2733–2755.

Piomelli, U., E. Balaras, and A. Pascarelli (2000), Turbulent structures in accelerating boundary layers, *J. Turbulence*, *1*, 001.

Piomelli, U., A. Scotti, and E. Balaras (2001), Large eddy simulation of turbulent flows, from desktop to supercomputer, in *Vector and Parallel Processing—VECPAR 2000*, edited by J. M. L. M. Palma et al., pp. 551–577, Springer-Verlag, New York.

Ribberink, J., and A. Al-Salem (1994), Sediment transport in oscillatory boundary layers in cases of rippled beds and sheet flow, *J. Geophys. Res.*, *99*, 12,707–12,727.

Scotti, A., and U. Piomelli (2001), Numerical simulation of pulsating turbulent channel flow, *Phys. Fluids*, *13*(5), 1367–1384.

Scotti, A., and U. Piomelli (2002), Turbulence models in pulsating flows, *AIAA J.*, *40*(3), 537–544.

Sleath, J., and S. Wallbridge (2002), Pickup from rippled beds in oscillatory flow, *J. Waterw. Port Coastal Ocean Eng.*, *128*(6), 228–237.

Sumer, B. M., and R. Deigaard (1981), Particle motions near the bottom in turbulent flow in an open channel. Part 2, *J. Fluid Mech.*, *109*, 311–337.

Sumer, B. M., and B. Oğuz (1978), Particle motions near the bottom in turbulent flow in an open channel, *J. Fluid Mech.*, *86*, 109–127.

Sumer, B., A. Kozakiewicz, J. Fredsœ, and R. Deigaard (1996), Velocity and concentration profiles in sheet-flow layer of movable bed, *J. Hydraul. Eng.*, *122*(10), 549–558.

Thorne, P. D., J. J. Williams, and A. G. Davies (2002), Suspended sediments under waves measured in a large-scale flume facility, *J. Geophys. Res.*, *107*(C8), 3178, doi:10.1029/2001JC000988.

Vittori, G. (2003), Sediment suspension due to waves, *J. Geophys. Res.*, *108*(C6), 3173, doi:10.1029/2002JC001378.

Wikramanayake, P. N. (1993), Velocity profiles and suspended sediment transport, Ph.D. thesis, Dept. of Civil and Environ. Eng., Mass. Inst. of Technol., Cambridge, Mass.

Wilcox, D. C. (1998), *Turbulence Modeling for CFD*, 2nd ed., DCW Ind., La Cañada, Calif.

Yalin, M. S. (1977), *Sediment Transport*, Pergamon, New York.

Zedler, E., and R. Street (2001), Large-eddy simulation of sediment transport: Current over ripples, *J. Hydraul. Eng.*, *127*(6), 444–452.

Zedler, E. A., and R. L. Street (2002), Nearshore sediment tranport: Unearthed by large eddy simulation, in *Coastal Engineering 2002: Solving Coastal Conundrums*, edited by J. M. Smith, pp. 2504–2515, World Sci., River Edge, N. J.

Y. S. Chang, Department of Meteorology and Physical Oceanography, Rosenstiel School of Marine and Atmospheric Science, University of Miami, Miami, FL 33149, USA. (yschang@rsmas.miami.edu)

A. Scotti, Department of Marine Sciences, University of North Carolina, Chapel Hill, NC 27599, USA. (ascotti@unc.edu)